Inclusion Characteristics and Acicular Ferrite Nucleation in Ti-Containing Weld Metals of X80 Pipeline Steel

BINGXIN WANG, XIANGHUA LIU, and GUODONG WANG

X80 steel weld metals with Ti contents of 0.003 to 0.13 pct were prepared by the single-pass submerged-arc welding process. The effects of Ti content in weld metals on the constituent phases of inclusions and chemical compositions of the constituent phases, as well as the potency of acicular ferrite (AF) nucleation on the inclusions were investigated. Moreover, the crystallographic orientation relationship between the AF and inclusion was examined. The results show that with an increase in Ti content, the primary constituent phases of the inclusions change from the (Mn-Al-Si-O) compound to a mixture of spinel and pseudobrookite solid solutions, and eventually to pseudobrookite. The spinel solid solution is characterized by the $MnTi_2O_4$ constituent. Compared to pseudobrookite, spinel has a lower Ti concentration, but a significantly higher Mn content. In the case of the presence of a considerable amount of spinel, the Mn element is enriched strongly in the inclusions, resulting in the development of a Mn-depleted zone (MDZ) in the matrix around the inclusions, which enhances the driving force for AF formation. AF shows the Baker–Nutting orientation relationship with $MnTi_2O_4$. The formation of MDZ and the presence of the Baker–Nutting orientation relationship promote the ability of inclusions to nucleate the intragranular AF.

https://doi.org/10.1007/s11661-018-4570-y

I. INTRODUCTION

HIGH-STRENGTH low-alloy (HSLA) steels, such as the X80 pipeline steel, have been widely used in the constructions of long-distance oil and gas transportation systems, offshore structures, vessels, and other structures, due to their excellent combination of strength and toughness. However, the impact toughness of the weld metals tends to deteriorate after the welding thermal cycle because of the formation of coarse grain boundary allotriomorphic ferrite and well-aligned side plate ferrite (*i.e.*, Widmanstätten) in the microstructures of the weld metals. A chaotic arrangement of laths and fine-grained interlocking microstructural characteristics of acicular ferrite (AF) can effectively retard crack propagation, noticeably improving the toughness.[1–3] Thus, AF is expected to develop fully in the microstructures of weld metals.

The fine interlocking AF nucleates intragranularly in the form of separate laths on non-metallic inclusions, and competes with the grain boundary ferrite (*i.e.*, Widmanstätten and lath bainite) during the austenite to ferrite transformation.[4] Hence, the factors controlling the AF formation mainly include prior austenite grain size, density and size of inclusions, and chemical compositions of the steels and/or weld metals.[4–8] However, the most essential condition is the ability of inclusions to nucleate the intragranular AF. Among some non-metallic inclusions, such as titanium nitride, vanadium nitride, and manganese sulfide, Ti-containing inclusions in particular have been known to strongly promote the formation of AF microstructure, and many studies have been performed to investigate the behavior and mechanisms of the Ti-containing inclusions inducing ferrite nucleation. Yamada *et al.*[9] and Takada *et al.*[10] pointed out that the TiO phase on the inclusions' surface contributes to the heterogeneous nucleation of AF and that the AF nucleated on TiO shows the Baker–Nutting (B–N) orientation relationship with the TiO. This orientation relationship achieves good lattice coherency and decreases the interfacial energy between the AF and TiO, resulting in a decrease in activation energy for AF nucleation. Nako *et al.*[11] and Kang *et al.*[12] found that $MnTi_2O_4$ on the surfaces of the inclusions is responsible for the formation of AF. In

BINGXIN WANG is with College of Mechanical Engineering, Liaoning Shihua University, Fushun 113001, China. Contact e-mail: wangbingxin@163.com. XIANGHUA LIU and GUODONG WANG are with the State Key Laboratory of Rolling & Automation, Northeastern University, Shenyang 110004, China.
Manuscript submitted August 2, 2017.
Article published online March 9, 2018

their studies, it was revealed that AF can have not only the B–N orientation relationship with $MnTi_2O_4$ but also the Kurdjumov–Sachs (K–S) orientation relationship with the austenite matrix. Formation of both B–N and K-S orientation relationships lowers the AF/$MnTi_2O_4$ and AF/austenite interfacial energies, giving rise to the AF nucleation.

More recently, the Mn depletion phenomenon has attracted much attention. Several researchers[13–18] have reported that a Mn-depleted zone (MDZ) can be detected around Ti_2O_3 inclusions in steels and weld metals, so that the local depletion of Mn around the inclusions promotes ferrite nucleation by increasing the chemical driving force. Shim *et al.*[19] also proved the above results in a steel-Ti_2O_3 diffusion bonding experiment. Regarding the mechanism by which the Ti-containing inclusions promote MDZ formation, Shim *et al.*[17] explained that Ti_2O_3 particles have a high concentration of cation vacancies and that the ionic radii of Mn^{+3} and Ti^{+3} ions are almost identical. Thus, Ti_2O_3 particles can absorb Mn atoms from the surrounding matrix without inducing a severe lattice distortion in the Ti_2O_3 structure, giving rise to a narrow MDZ in close proximity to Ti_2O_3 inclusions.

However, for the Mn depletion effect, Kang *et al.*[20,21] proposed an entirely different concept based on the investigation of Mn depletion behavior in high-strength low-alloy steel weld metals. Their studies have found no MDZ formation around inclusions mainly composed of Ti_2O_3. On the contrary, in the presence of Mn-enriched inclusions containing large amounts of $MnTi_2O_4$ and $MnTiO_3$ constituents, the Mn in the matrix around the inclusions is consumed, and as a result, the MDZ is developed. Jiang *et al.*[22] also reached similar conclusions in their investigation of microstructure refinement and mechanical properties improvement by developing intragranular acicular ferrite (IAF) on inclusions in the Ti-Al complex deoxidized HSLA steel. It is also worth noting that, in contrast to Kang's experimental results, Nako *et al.*[11] did not find the MDZ around the inclusions containing the $MnTi_2O_4$ constituent in their studies of crystal orientation relationships between the AF, oxide, and the austenite matrix in low-carbon steel submerged-arc welding weld.

As can be seen from the studies mentioned above, disagreements and even contradictory ideas still exist regarding the behavior and mechanism of Mn depletion caused by Ti-containing inclusions. Thus, it is still necessary to perform further investigations of the inclusions inducing AF nucleation. Although the phenomenon of AF nucleation on Ti-containing inclusions has been well demonstrated in the literature, few studies have systematically investigated the variation of the constituent phases of the inclusions, especially the chemical compositions of constituent phases, with the Ti content in weld metals. The present work focuses on the constituent phases and chemical composition characteristics of the constituent phases, as well as the relationships between the chemical composition features of the constituent phases and the Mn depletion behavior in order to further elucidate the Mn depletion mechanism. In addition, the crystallographic orientation relationship between the AF and the inclusion was also investigated.

II. EXPERIMENTAL PROCEDURE

A. *Weld Metals Preparation*

X80 pipeline steel plates with dimensions of 200 × 100 × 20 mm and 60 deg single side V-groove served as the base metal. A single-pass submerged-arc welding process and a Ti-free C-Mn steel welding wire with a diameter of 4 mm were used under a voltage of 35 V, current of 450 A, welding speed of 0.32 cm/s, and heat input of 44.3 kJ/cm. Three weld metals with different Ti contents were obtained by adding different amounts of Ti-Fe powder with approximately 33 pct Ti to the groove prior to welding. Meanwhile, small amounts of Ni-Fe powder (99 pct Ni), Mo-Fe powder (55 pct Mo), and Mn-Fe powder (81 pct Mn) were also filled in order to prevent the formation of a considerable amount of the allotriomorphic polygonal ferrite in the microstructures of weld metals. The chemical compositions of the weld metals were analyzed using a Shimadzu OES-5500 optical emission spectrometer with the exception of nitrogen and oxygen, which were analyzed by a Leco TC-436 N/O analyzer. The chemical compositions of the welding consumables and weld metals are listed in Tables I and II, respectively. As shown in Table II, with the exception of Ti with a range of 0.003 to 0.13 pct, other elements such as carbon, silicon, manganese, and so on, maintained nearly constant concentrations. In light of the Ti content, weld metals were labeled as W30 (0.003 pct Ti), W200 (0.02 pct Ti), and W1300 (0.13 pct Ti).

B. *Inclusion Analyses and Examination of MDZ*

The specimens were cut from the weld metals, and examination planes perpendicular to the welding direction were prepared by mechanical polishing followed by etching with 4 pct nital solution. The metallographic microstructures were observed using a Leica DMIRM image analyzer. The morphology and chemical compositions of the inclusions were analyzed by a JEOL JXA-8530F electron probe micro-analyzer (EPMA) under scanning electron microscopy (SEM) and energy dispersive spectroscopy (EDS) modes, respectively. The slices with 0.3 mm thickness machined along the examination planes of the above specimens were mechanically thinned to 80 μm, followed by twin-jet electropolishing in an electrolyte of 8 pct perchloric acid and 92 pct ethanol at the temperature of −30 °C. The thin foils were examined on an FEI Tecnai G2 F20 scanning transmission electron microscope (STEM) equipped with an energy dispersive spectrometer under the accelerating voltage of 200 kV and line scanning mode in order to study the variation of Mn element across the inclusions and the surrounding matrix. Moreover, the driving force for AF nucleation was calculated with Thermo-Calc 3.0.1 using TCS Steels/Fe-alloys Database

Table I. Chemical Compositions of the Base Plate and Welding Wire (Mass Percent)

Materials	C	Mn	Si	Ni	Cr	Mo	S	P	Al	Nb	Ti
Base material	0.04	1.80	0.22	0.35	0.30	0.28	0.002	0.01	0.03	0.09	0.01
Welding wire	0.05	0.86	0.06	—	—	—	0.022	0.02	0.01	—	—

Table II. Chemical Compositions of Weld Metals (Mass Percent)

C	Mn	Si	Ni	Cr	Mo	S	P	Al	O	N	Ti
0.064	1.36	0.35	0.36	0.14	0.30	0.013	0.032	0.015	0.039	0.0037	0.003
0.061	1.41	0.36	0.38	0.15	0.31	0.012	0.032	0.017	0.035	0.0041	0.02
0.07	1.38	0.35	0.35	0.15	0.29	0.014	0.028	0.015	0.030	0.0039	0.13

Version 7.0 (TCFE 7) in order to illustrate the effect of the MDZ on the intragranular AF nucleation.

C. *Thermochemical Computing on the Formation of Inclusion*

The commercial thermochemical computing package FactSage™ (version 6.4) was employed to calculate the thermodynamic stability of various inclusion phases based on the Gibbs free energy minimization principle using the FToxid (for the oxide) and FSstel (for the steel) databases. Considering the high cooling rate after welding, on the basis of calculations of the equilibrium compositions of liquid oxides at 1600 °C for the above chemical compositions of weld metals, the Scheil–Gulliver cooling mode was applied to predict the formation of inclusions from the equilibrium constituents of molten oxides at 1600 °C.[20]

D. *Crystal Orientation Analysis Between inclusion and AF*

Transmission electron microscopy (TEM) analysis was conducted to investigate the inclusion/AF crystal orientation relationship using selected area electron diffraction patterns (SADP). Thin foil specimens for TEM analysis were prepared by the above-mentioned twin-jet polishing procedures followed by several ion milling steps, and were examined using an FEI Tecnai G2 F20 at an operating voltage of 200 kV.

III. RESULTS AND DISCUSSION

A. *Metallographic Microstructures of Weld Metals and EPMA Analyses of Inclusions*

Figure 1 shows the microstructural variation with Ti content in the weld metals. It can be seen that the AF amount is increased noticeably while the side plate and bainitic ferrites almost disappear as the Ti content changes from 0.003 to 0.02 pct (Figures 1(a) through (c)). The microstructure of the weld metal is completely composed of bainitic ferrite accompanied by the disappearance of AF with a further increase in the Ti content to 0.13 pct (Figure 1(d)). Therefore, Ti content strongly affects the weld metal microstructures.

Figures 2, 3, and 4 present the EPMA analysis results of the inclusions in the weld metals containing different amounts of Ti. In W30, the inclusion can not act as an effective nucleant for AF. A classic example is shown in the square region surrounded by green solid lines in the SEM image in Figure 2. According to chemical composition characteristics displayed in EPMA maps of the inclusion in Figure 2, the inclusion is mainly composed of the (Mn-Si-Al)-oxide accompanied by small amounts of (Mn-Ti)-oxide and discrete MnS patches distributed at the periphery of the inclusion.

In W200, examination of a typical inclusion in the marked region in the SEM image in Figure 3 clearly shows that several AF plates emanate from the surface of an inclusion, indicating that the inclusion has the ability to induce AF nucleation. In addition, the SEM image clearly shows that the inclusion contains two types of different colors of light and dark constituents. Comparison between the SEM image and EPMA maps of the inclusion shows that some elements' distribution, especially Si, Al, and Ti, correspond well to light and dark color constituents in the inclusion. More specifically, the light color constituent contains a higher level of Ti but is lower in Si and Al contents and should belong to (Mn-Ti)-oxide. Dark color one has the opposite chemical composition characteristics, so that it should be (Mn-Si-Al)-oxide. Similar to W30, some discrete MnS patches are also found to appear in the outer region of the inclusion. Compared to the inclusion in W30, the amount of (Mn-Ti)-oxide in the inclusion of W200 is remarkably increased at the expense of (Mn-Si-Al)-oxide. It is particularly worth noting that by comparisons of the Ti and Mn concentrations in the (Mn-Ti)-oxide marked as C1 with those in the (Mn-Ti)-oxide labeled as C2, there are two kinds of (Mn-Ti)-oxides differing in the Mn and Ti contents in the inclusion of W200, namely, one has a much higher Mn content but a lower Ti content (*i.e.*, C1), while the other has the opposite chemical composition characteristics with regard to the Ti and Mn element concentrations (*i.e.*, C2).

It can be seen from the marked region in the SEM image in Figure 4 that the inclusion in W1300 is inefficient for AF nucleation. As shown from EPMA maps, with the exception of a slight Mn enrichment caused by the presence of MnS in several locations on

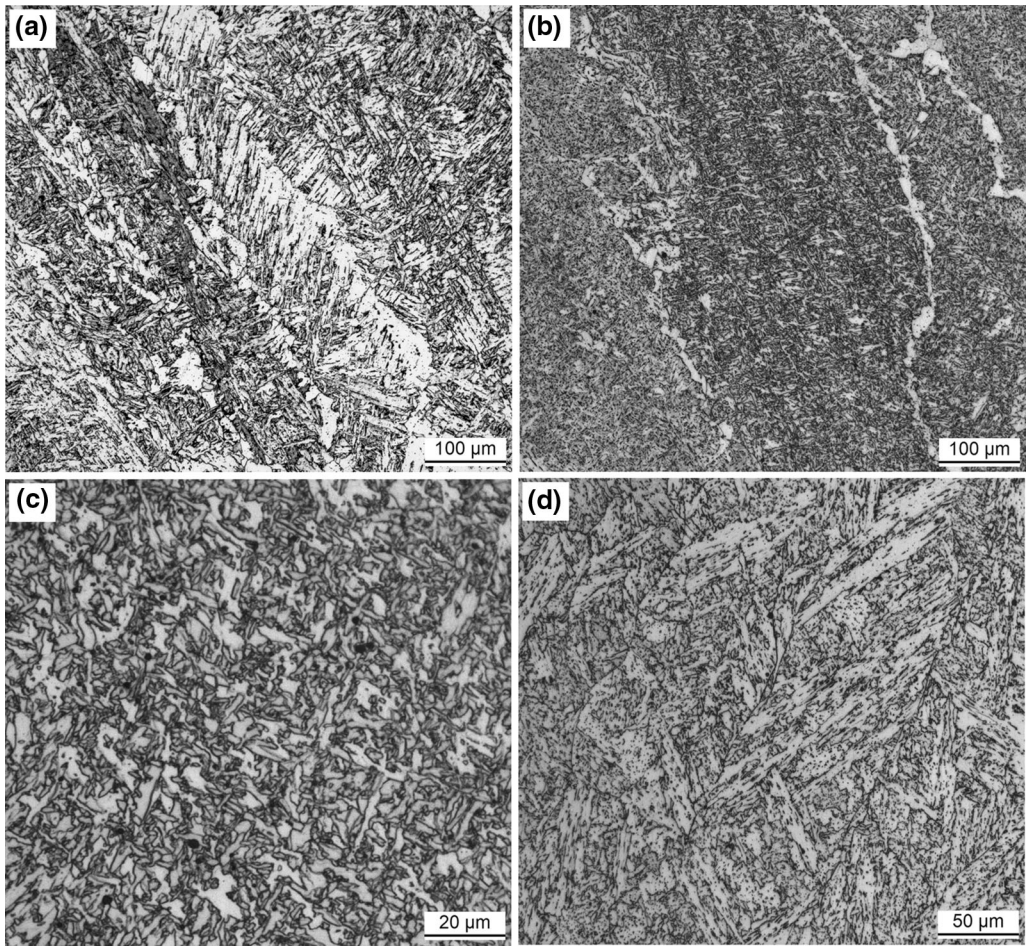

Fig. 1—Metallographic microstructures of (*a*) W30, (*b*) W200, (*c*) W200 under amplification, and (*d*) W1300.

the inclusion surface, the Mn and Si element contents in the inclusion are lower than those of the matrix located near the inclusion. Due to the absence of Mn and Si, the inclusion predominantly consists of Ti- and Al-oxides, and does not contain either (Mn-Si-Al)-oxide or (Mn-Ti)-oxide. Moreover, EPMA maps of the inclusion also show a much lower amount of MnS distributed at the periphery of the inclusion in W1300 than in W30 and W200. Studies in the literature[23–26] reported that liquid (Mn-Si-Al)-oxide shows high sulfur solubility, and during cooling, MnS starts to precipitate from the liquid oxide due to the decrease in the sulfur solubility. In other words, MnS precipitation is related to (Mn-Si-Al)-oxide. As previously mentioned, the inclusions in W30 and W200 have more (Mn-Si-Al)-oxide, while those in W1300 do not contain this phase, which results in the above difference in the amount of the MnS phase present in the inclusions.

Figure 5 shows EPMA spot analyses of the major constituents in the above inclusions (examination locations are marked at the inclusions). Examination of Figures 5(a) through (c) shows that (Ti-Mn)-oxide such as C1 in Figure 3 contains a higher Mn content than (Mn-Si-Al)-oxide. Moreover, Figure 5(d) indicates that the Ti-oxide constituent contains a very high concentration of Ti.

B. *Thermodynamic Calculations on Evolution of Inclusions*

Thermodynamic analyses of inclusion evolution and precipitation are presented in Figure 6. For the present chemical compositions of weld metals, the various phases involved in thermodynamic calculation are the slag phase, some types of solid solutions and $Mn_3Al_2Si_3O_{12}$ and $Mn_2Al_4Si_5O_{18}$ compounds. The slag phase is Al_2O_3-SiO_2-MnO-Ti_2O_3-TiO_2-FeO multi-component liquid oxide formed by deoxidation reactions of several elements in weld metals. Solid solutions include corundum, spinel, ilmenite, and pseudobrookite. Corundum is an Al_2O_3-rich phase with a limited solubility of Ti_2O_3, while spinel, pseudobrookite, and ilmenite are respectively composed of $MnTi_2O_4$-$FeTi_2O_4$-$MnAl_2O_4$-$FeAl_2O_4$, Ti_3O_5-$FeTi_2O_5$-$MnTi_2O_5$, and Ti_2O_3-$MnTiO_3$.

As demonstrated in Figure 6, corundum is formed prior to the other constituent phases of the inclusions during solidification of the liquid oxides, irrespective of the Ti content in the weld metals. This is because Al has

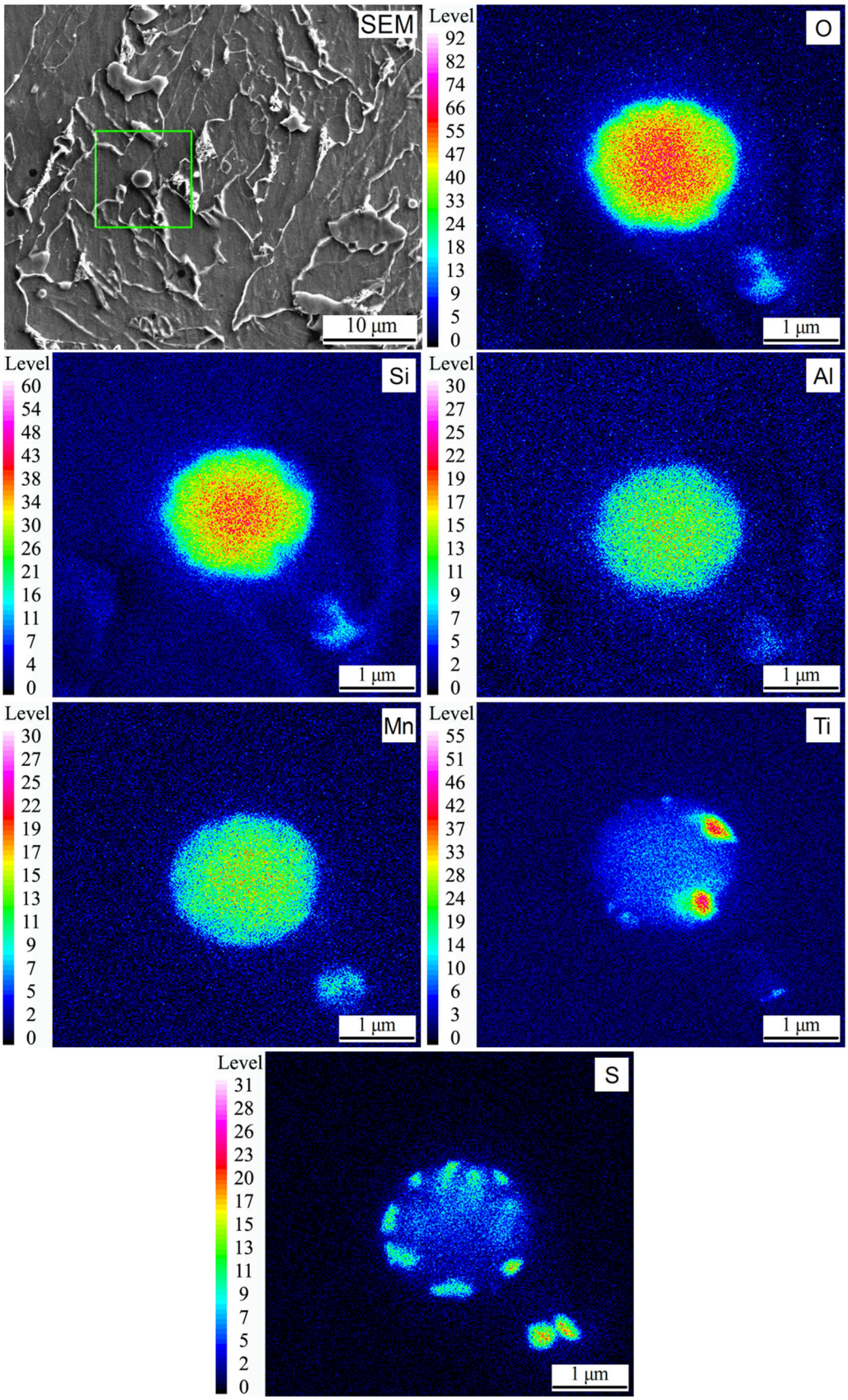

Fig. 2—SEM image and EPMA maps of the inclusion in W30.

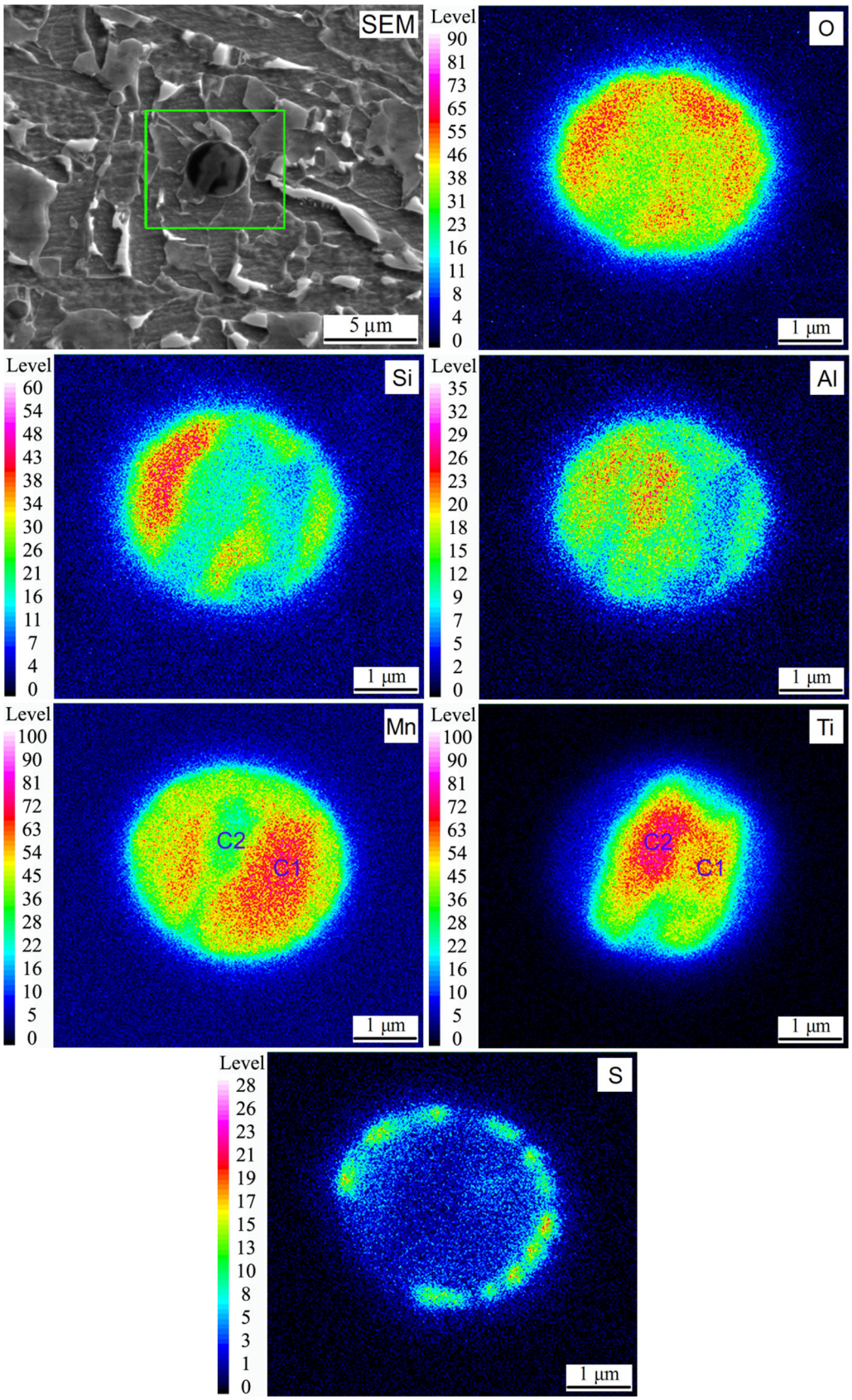

Fig. 3—SEM image and EPMA maps of the inclusion in W200.

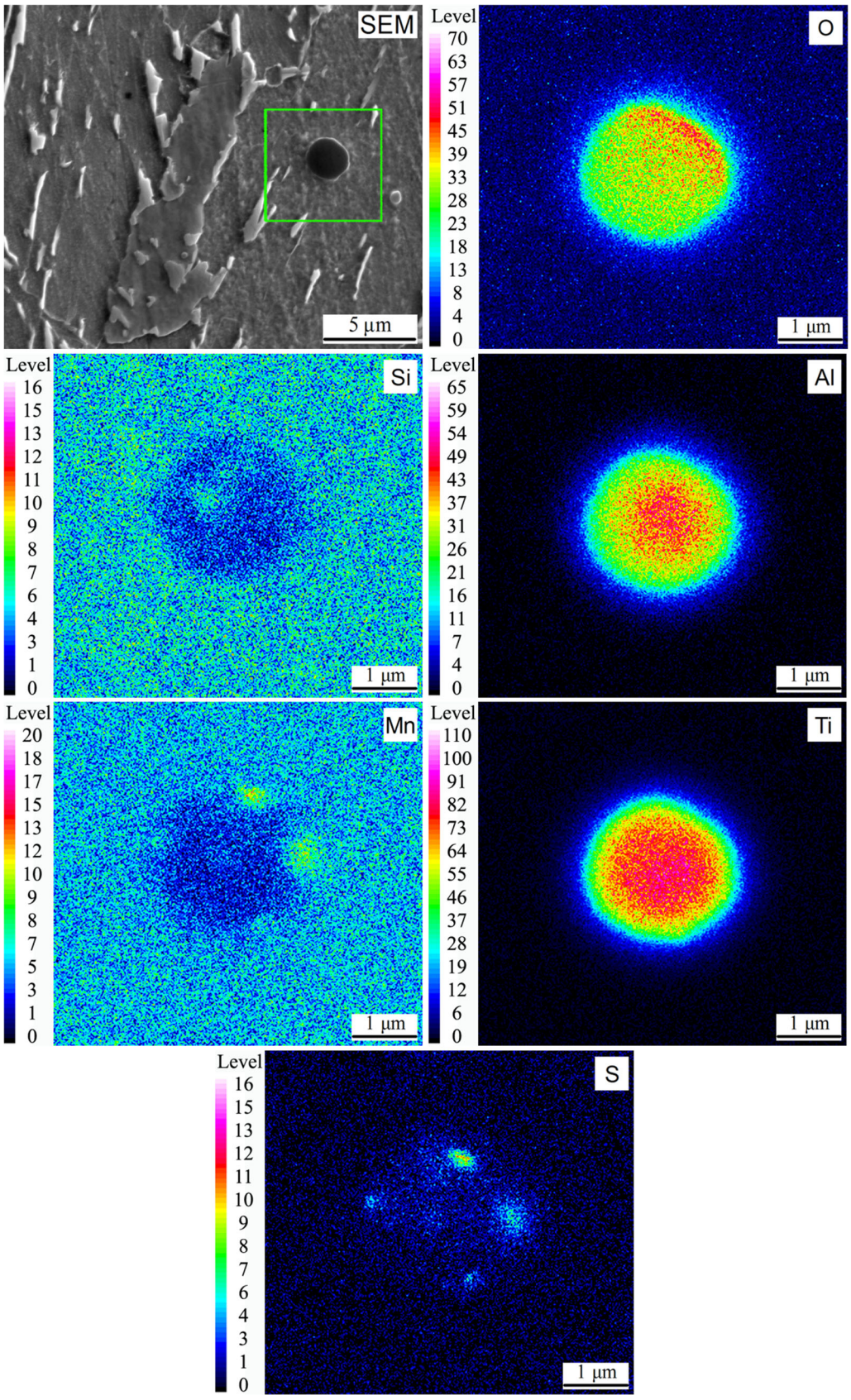

Fig. 4—SEM image and EPMA maps of the inclusion in W1300.

a greater oxygen affinity than Ti, Mn, Si, and Fe.[26] With an increase in the Ti content in weld metals, the precipitation temperatures of spinel and pseudobrookite are increased, while ilmenite becomes thermodynamically unstable. In addition, (Mn-Si-Al)-oxides (*i.e.*, $Mn_3Al_2Si_3O_{12}$ and $Mn_2Al_4Si_5O_{18}$) are usually precipitated from liquid oxides at a lower temperature range. Using selected area electron diffraction pattern (SADP) analysis, Seo *et al.*[15] proved that (Mn-Si-Al)-oxide is an amorphous phase.

It can be clearly observed from the constituent phases of the inclusions at 1000 °C (liquid oxides have been completely decomposed at this temperature) that, in W30, the inclusions are dominated by amorphous (Mn-Si-Al)-oxide. Moreover, the inclusions also contain a certain amount of corundum and small amounts of spinel, ilmenite, and pseudobrookite (Figure 6(a)). For W200, with the exception of the absence of ilmenite, the kinds of the constituent phases of inclusions are the same as those in W30, but the amounts of the different constituent phases are notably changed. Namely, the spinel and pseudobrookite contents are increased at the expense of (Mn-Si-Al)-oxide (Figure 6(b)). In W1300, the (Mn-Si-Al)-oxide phase disappears completely, and the inclusions contain a substantial amount of pseudobrookite, in addition to a certain amount of corundum and a minimal amount of spinel (Figure 6(c)).

It is worth noting that no MnS phase appears in the aforementioned thermodynamic calculations, even though MnS is frequently found to distribute in the outer region of inclusions in Figures 2, 3 and 4. As mentioned in the experimental procedures, two-stage consecutive thermodynamic calculations were performed, namely equilibrium compositions calculation of liquid oxides at 1600 °C and Scheil–Gulliver cooling analysis. Under chemical compositions of weld metals, the liquidus temperatures of weld metals are thermodynamically determined to be in the range of 1520 °C to 1550 °C. So the temperature of equilibrium composition calculation of liquid oxides (*i.e.*, 1600 °C) is above the liquidus temperatures of the weld metals, above which the supersaturation of sulfur is not sufficient to form sulfide.[27] As a result, the molten slags at 1600 °C do not contain MnS constituent, as shown in Table III,

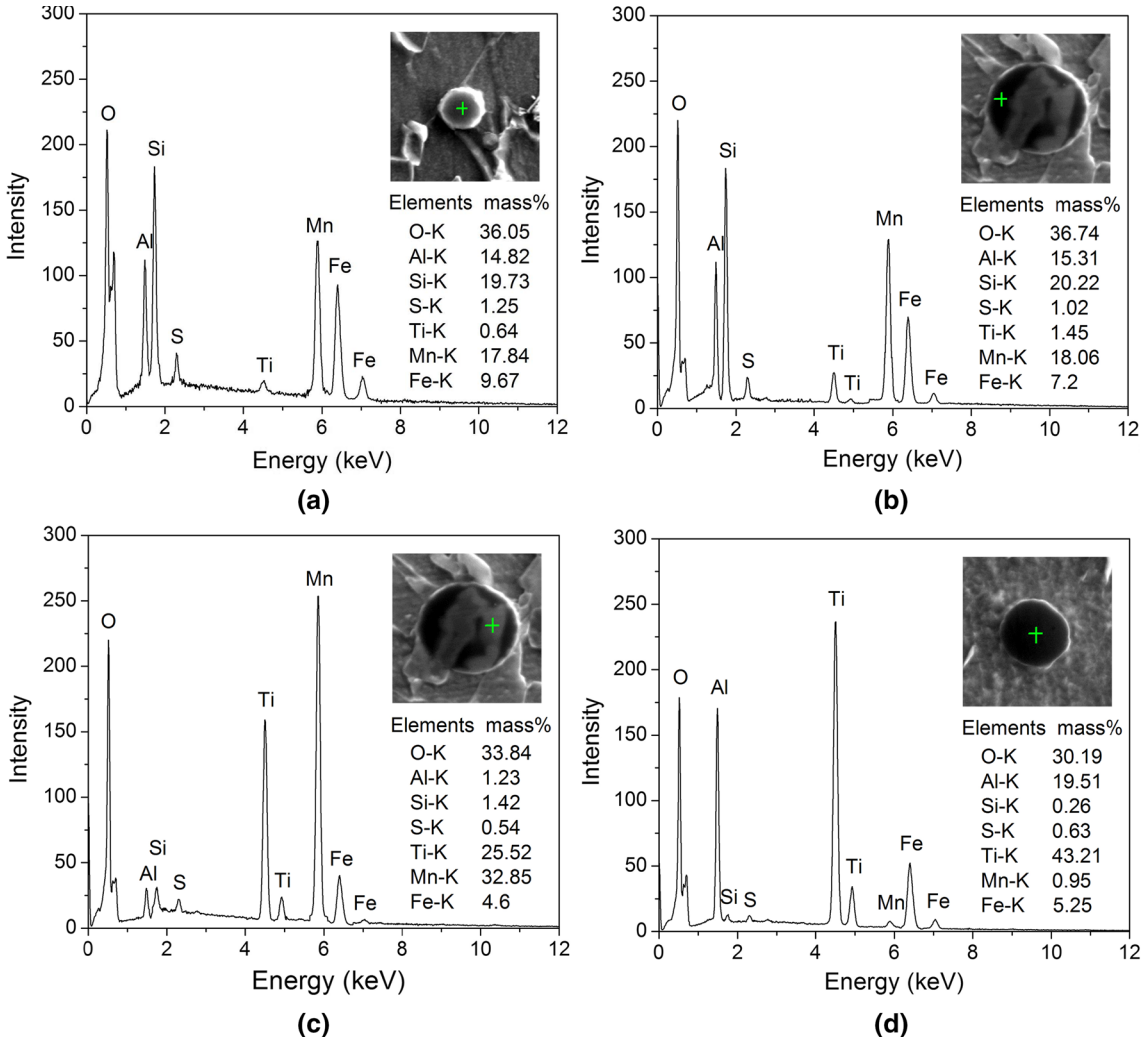

Fig. 5—EPMA spot analyses for (*a*) (Mn-Si-Al)-oxide in W30, (*b*) (Mn-Si-Al)-oxide in W200, (*c*) (Mn-Ti)-oxide in W200, and (*d*) Ti-oxide in W1300.

resulting in the absence of MnS in the inclusions predicted by the Scheil–Gulliver approach in conjunction with the equilibrium constituents calculation of molten oxides at 1600 °C.

The proportions of various solid solution constituents of the inclusions in weld metals with different Ti contents were obtained based on the thermodynamic calculation results and are shown in Figure 7. As the Ti content in weld metals is increased from 0.003 to 0.02 pct, the amount of $MnTi_2O_4$ constituent in spinel solid solution is significantly increased to a very high level. Further increase in the Ti content to 0.13 pct basically does not change the content of $MnTi_2O_4$ constituent (Figure 7(a)). For pseudobrookite solid solution, with an increase in the Ti content in weld metals, the proportion of Ti_3O_5 constituent is noticeably increased, accompanied by a drop in the content of $MnTi_2O_5$ constituent, so that in W1300 (*i.e.*, 0.13 Ti pct weld metal), pseudobrookite is nearly composed of single Ti_3O_5 constituent (Figure 7(b)). In corundum, the Al_2O_3 constituent maintains a very high content regardless of the Ti content in weld metals (Figure 7(c)).

A similar variation tendency of Mn, Ti and Al elements in solid solutions with Ti content in weld metals is shown in Figure 8 and is not described again. It is worth noting that although spinel and pseudobrookite are both Ti-rich solid solutions, spinel has a very high amount of Mn but a lower Ti content

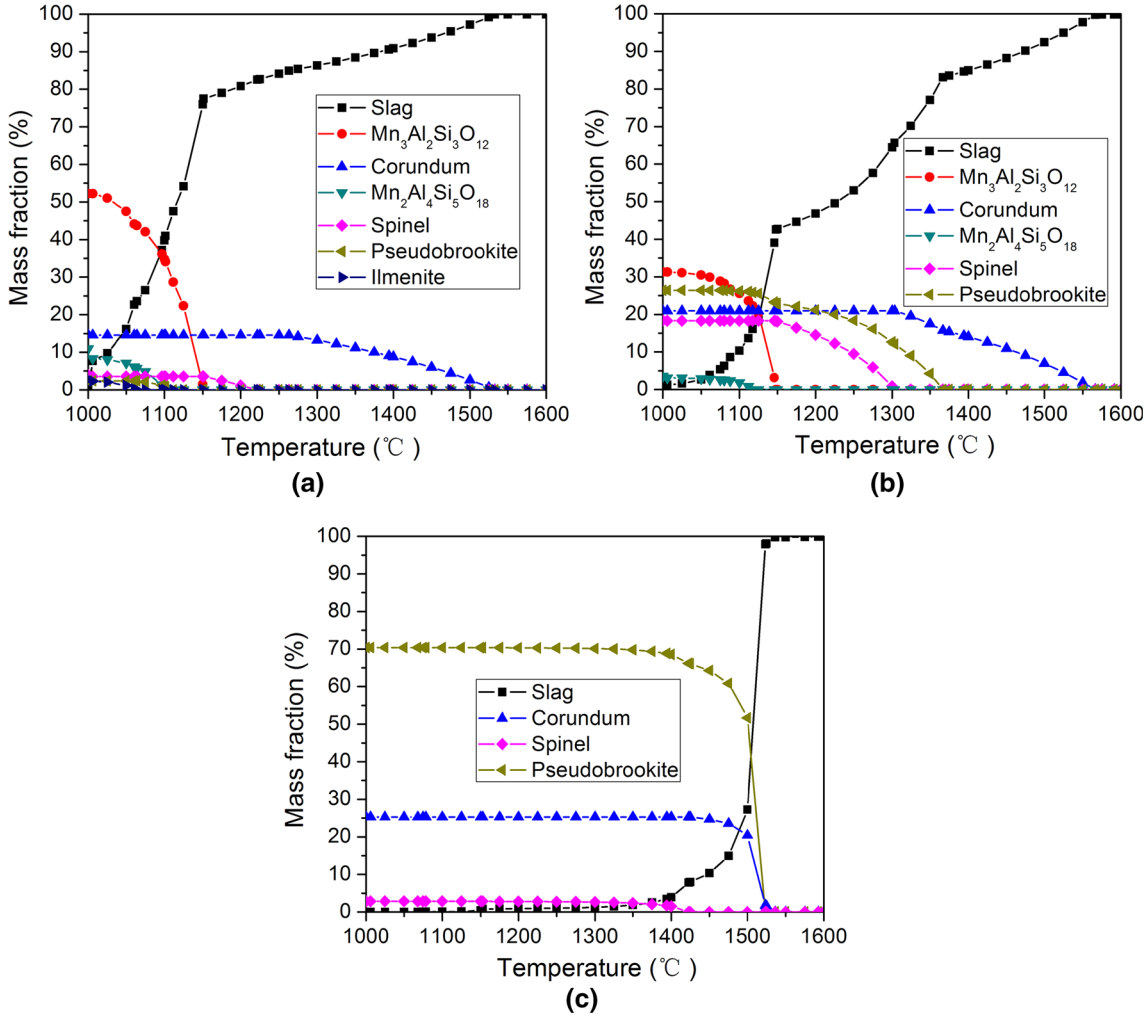

Fig. 6—Thermodynamic analyses of inclusion evolution for (*a*) W30, (*b*) W200, and (*c*) W1300.

Table III. Equilibrium Compositions of Liquid Oxides at 1600 °C (Mass Percent)

Weld metals	Al_2O_3	SiO_2	FeO	MnO	Ti_2O_3	TiO_2	[O]ppm
W30	34.87	30.1	3.1	28.16	1.93	1.79	39
W200	35.99	14.94	2.23	22.04	14.6	10.04	30
W1300	26.33	0.26	0.82	2.98	44.18	25.31	12

[O] represents the dissolved oxygen content in liquid weld metals at 1600 °C.

compared with pseudobrookite regardless of the Ti content in weld metals (Figures 8(a) and (b)).

Based on thermodynamic calculations, it is clear that (Mn-Si-Al)-oxides appearing in the EPMA analyses should be mainly the $Mn_3Al_2Si_3O_{12}$ compound, while the Ti-containing phases are undoubtedly spinel and pseudobrookite solid solutions. Additionally, thermodynamic calculation results can also provide a good explanation for the chemical composition characteristics of the inclusions exhibited in EPMA maps. As shown in Figures 6, 7, and 8, in W200, larger amounts of spinel and pseudobrookite simultaneously appear in the inclusions, and spinel has a higher Mn content but a lower Ti content, while pseudobrookite has the opposite chemical composition characteristics. As a result, as presented in Figure 3, there are two kinds of Ti-containing phases differing in the Ti and Mn concentration levels in the inclusions in W200; the phase with the higher Mn content is spinel (*i.e.*, C1 marked in Figure 3), while the other phase with the higher Ti content is pseudobrookite (*i.e.*, C2 marked in Figure 3). The thermodynamic calculation results also show that in W1300, the inclusions are mainly composed of pseudobrookite. Moreover, the spinel content in the inclusions is very low, and $Mn_3Al_2Si_3O_{12}$ compound is completely absent. At the same time, in W1300, pseudobrookite contains hardly any Mn but has a very high Ti content. Therefore, the inclusions exhibit the chemical composition characteristics shown in Figures 4 and 5(d), namely, a very high Ti content and the absences of Mn and Si in W1300.

EPMA analyses and thermodynamic calculations both show that the increase in the Ti content in the weld metals increases the amounts of the Ti-containing constituent phases at the expense of the (Mn-Si-Al)-oxide. It is well known that during welding, a series of complex metallurgical physico-chemical reactions are expected to occur in the weld pool. Elements such as Al, Ti, Si, and Mn can combine with soluble oxygen in the weld pool, resulting in the formation of various liquid oxides (*i.e.*, molten slag) above the liquidus temperatures of the slags and the decrease in the amount of the soluble oxygen in the weld pool. Competitive relationships between Al, Ti, Si, and Mn are present during the oxidation process. Compared to Si and Mn, Al and Ti have much stronger affinities for oxygen. Thus, as the Ti

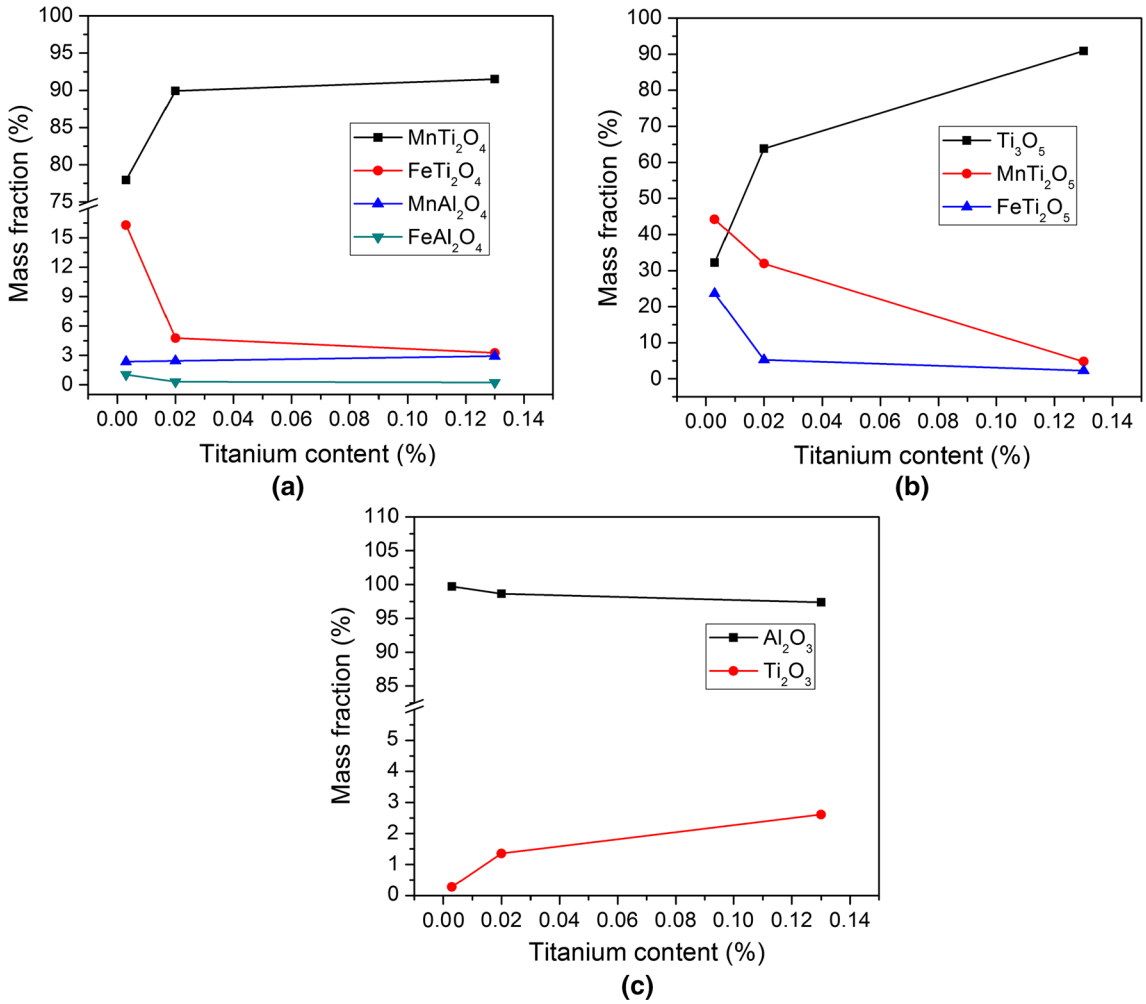

Fig. 7—Variations of constituent contents in (*a*) spinel, (*b*) pseudobrookite, and (*c*) corundum with Ti content in weld metals.

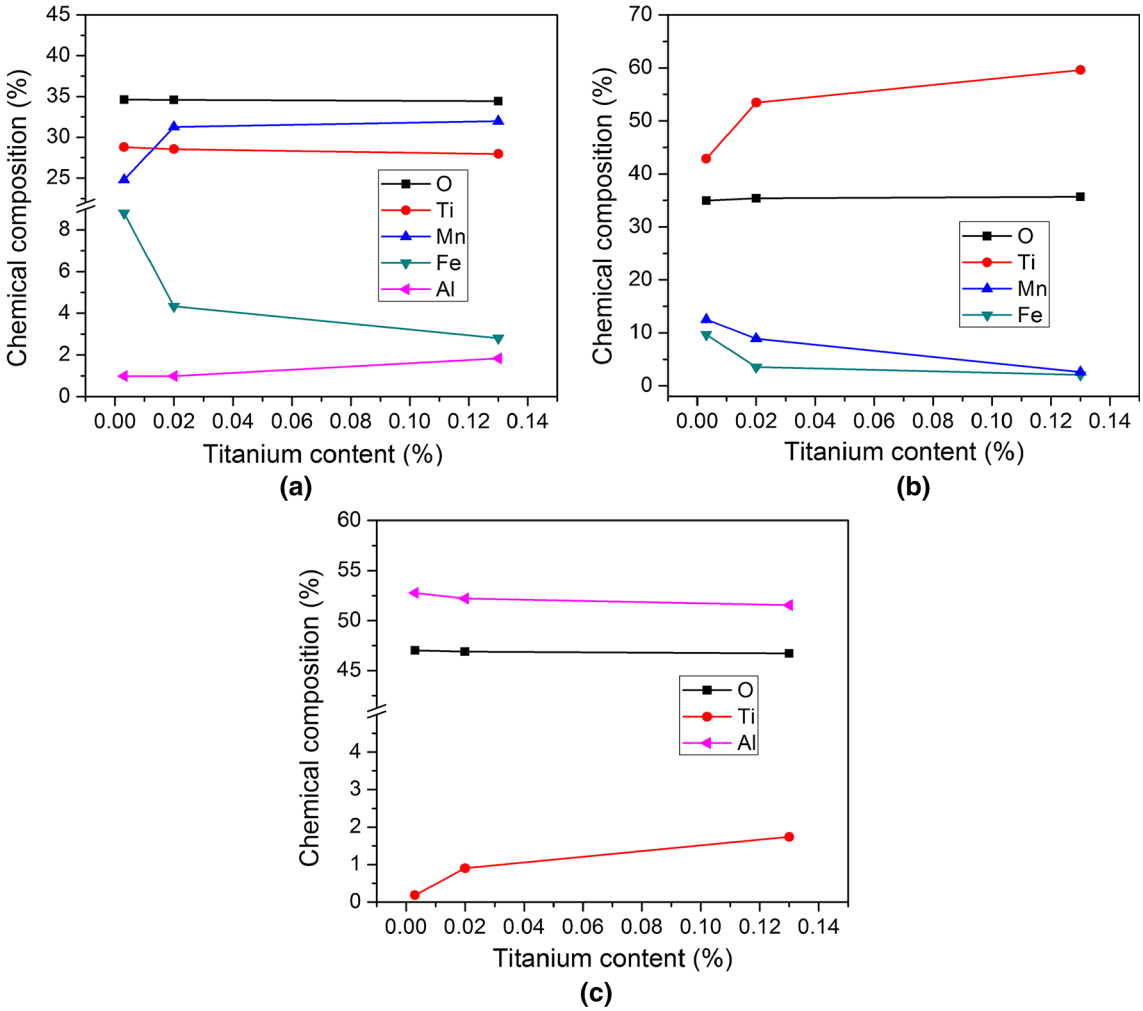

Fig. 8—Variations in chemical compositions of (*a*) spinel, (*b*) pseudobrookite, and (*c*) corundum with Ti content in weld metals.

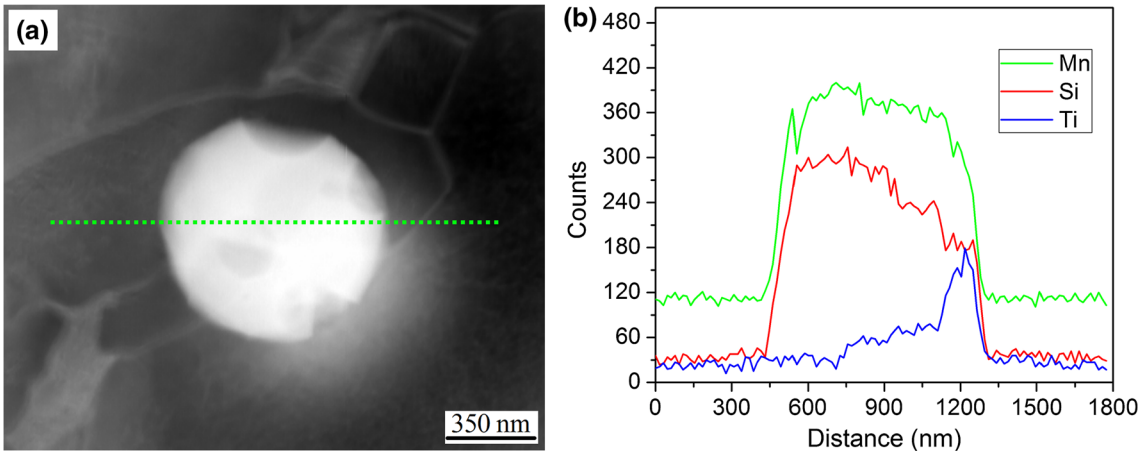

Fig. 9—EDS line scan analysis across an inclusion in W30 (*a*) STEM image with the trace of the line scan and (*b*) X-ray count profiles across the inclusion.

content is increased, Ti can combine with oxygen prior to Si and Mn to consume the soluble oxygen in the molten weld metals accompanied by an increase in the contents of the various titanium oxides (TiO_x). The decrease in the soluble oxygen in the molten weld metals is expected to suppress the oxidation reactions of Si and Mn,[27] leading to a decrease in the amounts of SiO_2 and MnO, as shown in Table III. During the post-welding

cooling, different kinds and amounts of constituent phases of the inclusions are expected to precipitate in light of the chemical composition characteristics of the liquid oxides. In the case of 0.003 pct Ti, the liquid oxide contains large amounts of SiO_2 and MnO constituents but very low amounts of Ti_2O_3 and TiO_2, resulting in a large amount of (Mn-Si-Al)-oxide accompanied by very low amounts of Ti-containing phases in the inclusions in W30. When the Ti content is increased to 0.02 pct, the amounts of SiO_2 and MnO constituents in the molten slag are decreased, but those of Ti_2O_3 and TiO_2 are correspondingly increased, causing an increase in the amounts of Ti-containing phases at the expense of (Mn-Si-Al)-oxide in the inclusions in W200. Under 0.13 pct Ti, the amounts of SiO_2 and MnO in the liquid oxide are very low, and in particular, the SiO_2 content is almost zero, resulting in the absence of (Mn-Si-Al)-oxide in the inclusions. Similarly, a very low content of MnO accompanied by a very high amount of TiO_x favors the formation of pseudobrookite rather than spinel. Thus, the inclusions in W1300 have a very high amount of pseudobrookite and a very low spinel content.

C. *MDZ Examination Around Inclusions*

As shown from the results presented in Figures 2, 3, and 4, the ability of the inclusions to nucleate intragranular AF is notably changed with Ti in the weld metals. The nucleation potency of the inclusions for intragranular AF was studied in view of the Mn depletion. For this purpose, STEM analysis in line scanning mode was used to examine the variation in manganese content in the vicinity of matrix/inclusion interfaces, as shown in Figures 9, 10, and 11. It is clearly evident that a distinct drop in the Mn content around the inclusion can be detected in W200 (Figure 10(b)), whereas no variations in the Mn concentration across the interface regions are found in W30 and W1300 (Figures 9(b) and 11(b)). With regard to the mechanism of Mn depletion, previous studies[17–19] have concluded that Mn absorption into Ti_2O_3 particles is responsible for the MDZ formation. However, in the present work,

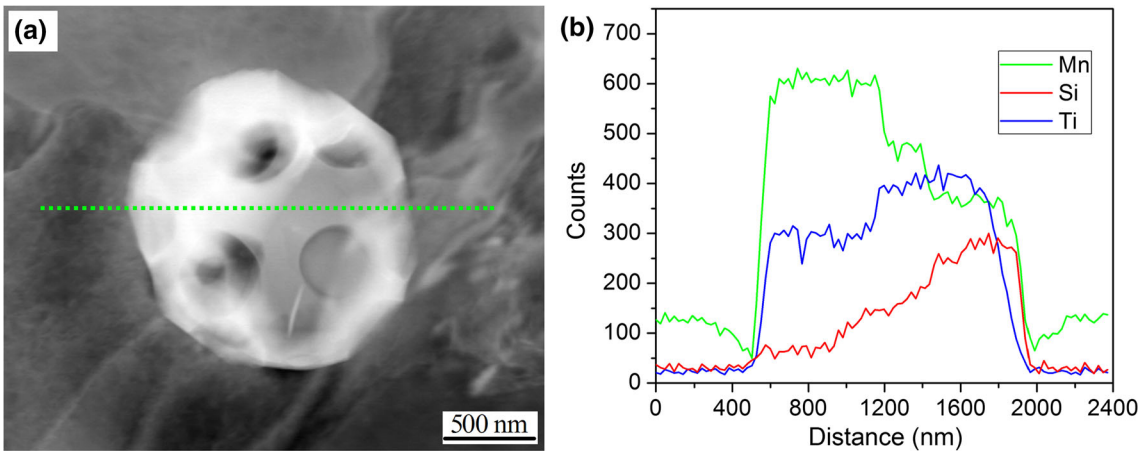

Fig. 10—EDS line scan analysis across an inclusion in W200 (*a*) STEM image with the trace of the line scan and (*b*) X-ray count profiles across the inclusion.

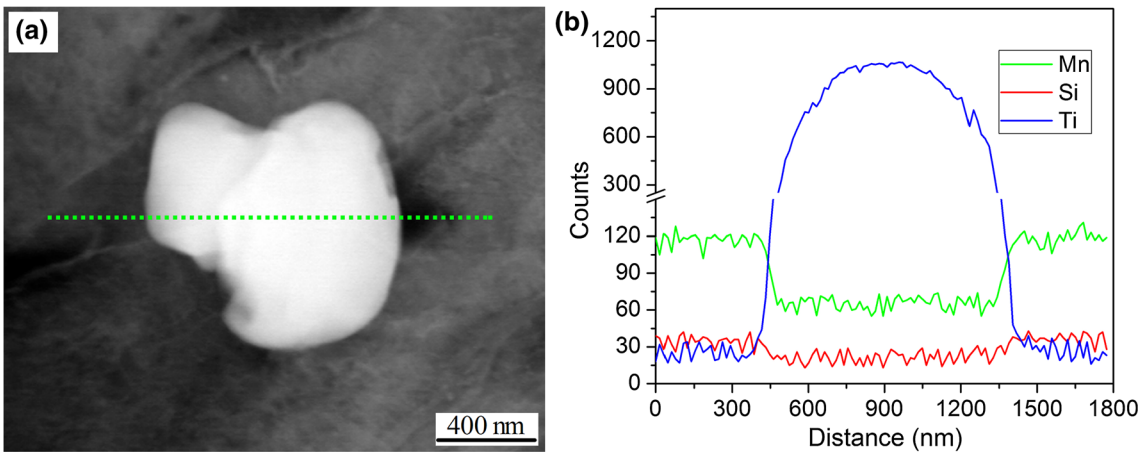

Fig. 11—EDS line scan analysis across an inclusion in W1300 (*a*) STEM image with the trace of the line scan and (*b*) X-ray count profiles across the inclusion.

the inclusions in W200 that give rise to Mn depletion do not contain any Ti_2O_3 constituent phases. Conversely, a larger amount of spinel dominated by $MnTi_2O_4$ is present in the inclusions, resulting in Mn enrichment in the inclusions. A strong Mn enrichment in the inclusions can remarkably consume the Mn in the surrounding matrix, leading to a drop in the Mn content in the matrix in the vicinity of the inclusions. Meanwhile, due to the high cooling rate after welding, the Mn content around the inclusions can not be recovered to the equilibrium state by long-range diffusion of Mn located far from the inclusions.[28] Thus, the MDZ is formed in the matrix adjacent to the inclusions. In W30, the inclusions predominantly consist of (Mn-Si-Al)-oxide with a lower Mn content. For W1300, the inclusions are characterized by pseudobrookite with Mn almost entirely absent. A lower Mn content or total absence of Mn in the inclusions is insufficient to form Mn depletion, resulting in the ineffectiveness of the inclusions for AF nucleation. In conclusion, the development of the MDZ is closely correlated with the presence of a large amount of Ti-containing and Mn-rich phases.

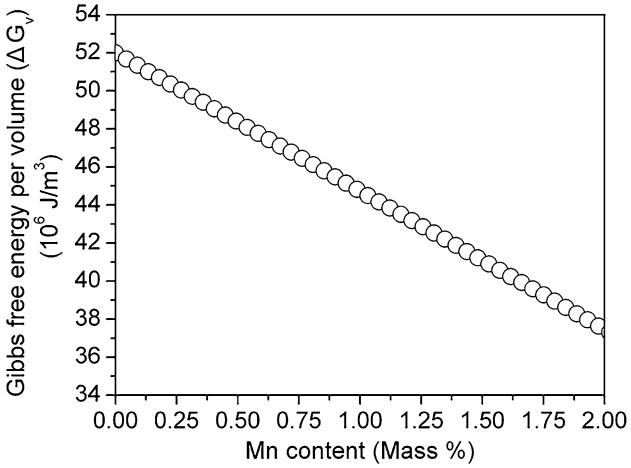

Fig. 12—Relationship between driving force for ferrite nucleation at 600 °C and Mn content.

To illustrate the contribution of the MDZ to intragranular nucleation, the driving force for ferrite formation (*i.e.*, the Gibbs free energy change per volume between austenite and ferrite) for different Mn contents is calculated with Thermo-Calc using the chemical

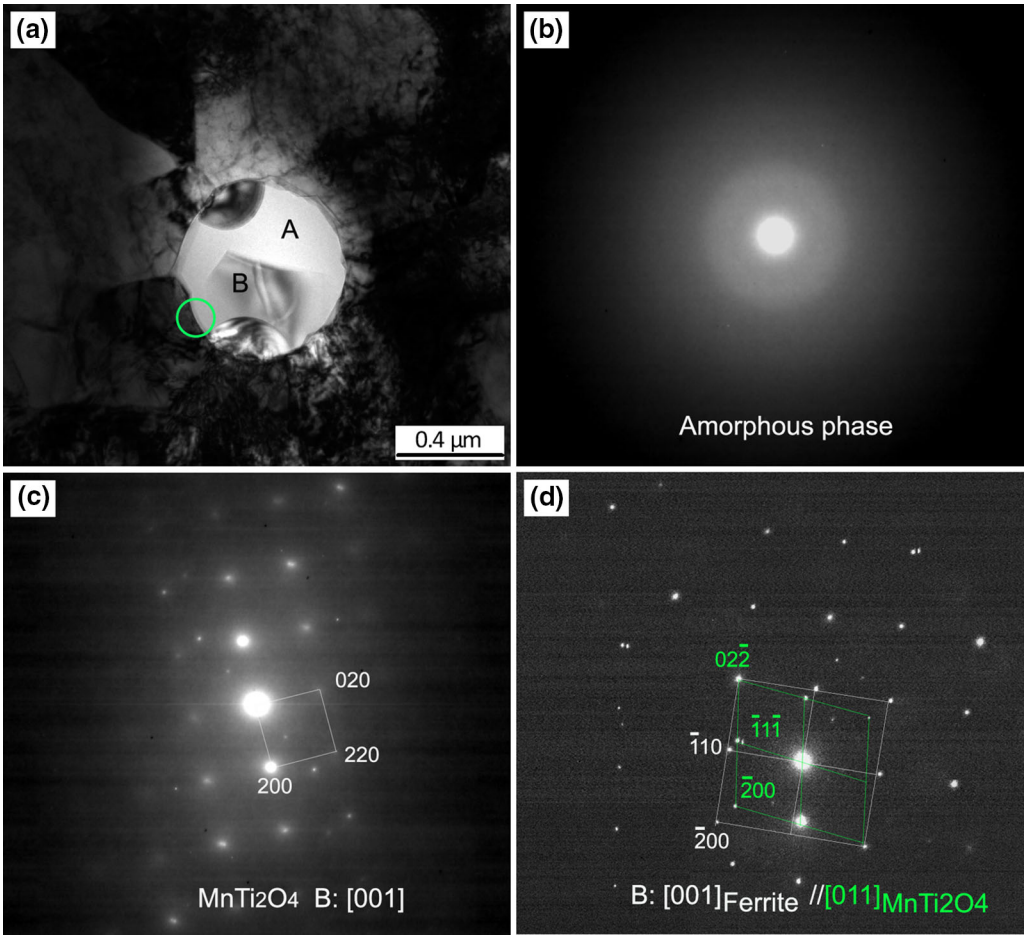

Fig. 13—Results of SADP analysis for the inclusion in W200: (*a*) bright field image of inclusion, (*b*) and (*c*) SADPs taken from regions A and B in (a), respectively, and (*d*) SADP of the circled area in (a).

compositions of W200 except for Mn, with the results shown in Figure 12. It can be clearly seen from Figure 12 that the driving force is increased with the decrease in Mn content (*i.e.*, Mn depletion), which increases the capability for intragranular AF nucleation on Ti-containing inclusions with the MDZ.

D. *Crystallographic Orientation Analysis between $MnTi_2O_4$ and AF*

In addition to the formation of the MDZ, the presence of a crystallographic orientation relationship is another generally accepted mechanism proposed for inducing the nucleation of IAF on inclusions. These two mechanisms are not mutually exclusive in many instances and depend substantially on the composition and structure of the inclusions. Accordingly, the orientation relationship between the nucleated AF and the inclusion in W200 was also investigated by SADP analysis, with the results shown in Figure 13. The halo pattern of Figure 13(b) and the identification result of Figure 13(c) demonstrate that the main constituent phases of the inclusion are amorphous (Mn-Si-Al)-oxide and $MnTi_2O_4$, in good agreement with the results described above. More importantly, it can be seen from the SADPs obtained from the interface of $MnTi_2O_4$ and adjacent AF shown in Figure 13(d) that the nucleated AF has the B–N orientation relationship of $(100)_{Ferrite}//(100)_{MnTi2O4}$ and $[001]_{Ferrite}//[011]_{MnTi2O4}$ with $MnTi_2O_4$, which is in accordance with the results reported in the literature.[11,12] The presence of low energy AF/$MnTi_2O_4$ interface with the B–N orientation relationship promotes intragranular AF formation by lowering the activation energy for AF nucleation.

Even though the AF nucleation could be controlled by complex factors, the present work reveals that the formation of the MDZ and the presence of the Baker–Nutting orientation relationship enhance the nucleation potency of the AF on inclusions in the weld metals.

IV. CONCLUSIONS

(1) The kinds and amounts of the constituent phases of the inclusions change remarkably with the Ti content in the weld metals. In the 0.003 pct Ti weld metal, the inclusions are mainly composed of amorphous (Mn-Si-Al)-oxide accompanied by a certain amount of corundum and small amounts of spinel, ilmenite, and pseudobrookite. In the 0.02 pct Ti weld metal, the amounts of spinel and pseudobrookite are increased at the expense of (Mn-Si-Al)-oxide. For the 0.13 pct Ti weld metal, the (Mn-Si-Al)-oxide phase disappears completely, and the inclusions contain a substantial amount of pseudobrookite, in addition to a certain amount of corundum and a minimal amount of spinel.

(2) $MnTi_2O_4$ is the primary constituent of spinel solid solution. The proportion of Ti_3O_5 in pseudobrookite is strikingly increased with the increase in Ti content accompanied by a drop in the content of the $MnTi_2O_5$ constituent. Compared to pseudobrookite, spinel has a lower Ti concentration but a significantly higher Mn content regardless of the Ti content in the weld metals.

(3) The development of the Mn-depleted zone is closely correlated with the presence of a large amount of Ti-containing and Mn-rich phases. In the 0.02 pct Ti weld metal, a high proportion of the spinel containing very high Mn amount can consume the Mn in the surrounding matrix, resulting in the formation of a Mn-depleted zone in the matrix in the vicinity of the inclusions. The predominantly (Mn-Si-Al)-oxide inclusions with the lower Mn content in the 0.003 pct Ti weld metal, or the pseudobrookite-dominated inclusions almost without Mn in the 0.13 pct Ti weld metal are insufficient for the formation of Mn depletion.

(4) Nucleated AF shows the B–N orientation relationship with $MnTi_2O_4$. The formation of the MDZ and the presence of the Baker–Nutting orientation relationship enhance the nucleation potency of AF on inclusions in the weld metals.

ACKNOWLEDGMENTS

This work was financially supported by the Project of Education Department of Liaoning Province (Grant No. L2016132). The authors are grateful to Drs. H.Y. Wu, W.N. Zhang (State Key Laboratory of Rolling & Automation of Northeastern University, China), and L.Z. Kong (School of Metallurgy of Northeastern University, China) for their help with EPMA and STEM analyses work as well as thermodynamic calculations.

REFERENCES

1. L. Zhang, Y.J. Li, J. Wang, and Q.L. Jiang: *ISIJ Int*., 2011, vol. 51, pp. 1132–36.
2. S.Y. Han, S.Y. Shin, S. Lee, N.J. Kim, J.H. Bae, and K. Kim: *Metall. Mater. Trans. A*, 2010, vol. 41A, pp. 329–40.
3. B.X. Wang and J.B. Lian: *Mater. Sci. Eng. A*, 2014, vol. 592, pp. 50–56.
4. J.L. Lee and Y.T. Pan: *ISIJ Int*., 1995, vol. 35, pp. 1027–33.
5. T.K. Lee, H.J. Kim, B.Y. Kang, and S.K. Hwang: *ISIJ Int*., 2000, vol. 40, pp. 1260–68.
6. Q.L. Jiang, Y.J. Li, J. Wang, and L. Zhang: *Mater Sci. Technol*., 2011, vol. 27, pp. 1385–90.
7. J. Hu, L.X. Du, and J.J. Wang: *Scripta Mater*., 2013, vol. 68, pp. 953–56.
8. W.Z. Mu, P.G. Jonsson, and K. Nakajima: *J. Mater. Sci*., 2016, vol. 51, pp. 2168–80.
9. T. Yamada, H. Terasaki, and Y.I. Komizo: *ISIJ Int*., 2009, vol. 49, pp. 1059–62.
10. A. Takada, Y.-I. Komizo, H. Terasaki, T. Yokota, K. Oi, and K. Yasuda: *Weld. Int*., 2015, vol. 29, pp. 254–61.

11. H. Nako, H. Hatano, Y. Okazaki, K. Yamashita, and M. Otsu: *ISIJ Int*., 2014, vol. 54, pp. 1690–96.
12. Y.J. Kang, S.H. Jeong, J.H. Kang, and C.H. Lee: *Metall. Mater. Trans. A*, 2016, vol. 47A, pp. 2842–54.
13. J.S. Seo, H.J. Kim, and C.H. Lee: *ISIJ Int*., 2013, vol. 53, pp. 880–86.
14. K. Yamamoto, T. Hasegawa, and J.I. Takamura: *ISIJ Int*., 1996, vol. 36, pp. 80–86.
15. K.Y. Seo, Y.M. Kim, H.J. Kim, and C.H. Lee: *ISIJ Int*., 2015, vol. 55, pp. 1730–38.
16. Y.B. Kang and H.G. Lee: *ISIJ Int*., 2010, vol. 50, pp. 501–508.
17. J.H. Shim, J.S. Byun, Y.W. Cho, Y.J. Oh, J.D. Shim, and D.N. Lee: *Scripta Mater*., 2001, vol. 44, pp. 49–54.
18. J.S. Byun, J.H. Shim, Y.W. Cho, and D.N. Lee: *Acta Mater*., 2003, vol. 51, pp. 1593–1606.
19. J.H. Shim, Y.W. Cho, S.H. Chung, J.D. Shim, and D.N. Lee: *Acta Mater*., 1999, vol. 47, pp. 2751–60.
20. Y.J. Kang, J.H. Jang, J.H. Park, and C.H. Lee: *Met. Mater. Int*., 2014, vol. 20, pp. 119–27.
21. Y.J. Kang, K.T. Han, J.H. Park, and C.H. Lee: *Metall. Mater. Trans. A*, 2014, vol. 45A, pp. 4753–57.
22. M. Jiang, X.H. Wang, Z.Y. Hua, K.P. Wang, C.W. Yang, and S.R. Li: *Mater. Charact*., 2015, vol. 108, pp. 58–67.
23. D.H. Woo, Y.B. Kang, H. Gaye, and H.G. Lee: *ISIJ Int*., 2009, vol. 49, pp. 1490–97.
24. H.S. Kim, H.G. Lee, and K.S. Oh: *Metall. Mater. Trans. A*, 2001, vol. 32A, pp. 1519–25.
25. H.S. Kim, H.G. Lee, and K.S. Oh: *ISIJ Int*., 2002, vol. 42, pp. 1404–11.
26. H.S. Kim, H.G. Lee, and K.S. Oh: *Met. Mater*., 2000, vol. 6, pp. 305–10.
27. K.C. Hsieh, S.S. Babu, J.M. Vitek, and S.A. David: *Mater. Sci. Eng. A*, 1996, vol. 215, pp. 84–91.
28. Y.J. Kang, K.T. Han, J.H. Park, and C.H. Lee: *Metall. Mater. Trans. A*, 2015, vol. 46A, pp. 3581–91.